Research Paper submitted to Journal of the Electrochemical Society

Title: Oxidative Dissolution of Tungsten Metal in Na_2CO_3 under $Ar–O_2–CO_2$ atmosphere

Author Names:
Kouji YASUDA,[1,2,3,*,z] Fumiyasu NOZAKI,[1] Ryotaro UEHATA,[1] and Rika HAGIWARA,[1,*]

Affiliation(s):
[1] Department of Fundamental Energy Science, Graduate School of Energy Science, Kyoto University, Yoshida-honmachi, Sakyo-ku, Kyoto 606-8501, Japan.
[2] Agency for Health, Safety and Environment, Kyoto University, Yoshida-honmachi, Sakyo-ku, Kyoto 606-8501, Japan.
[3] Present address: Department of Materials Science and Engineering, Graduate School of Engineering, Kyoto University, Yoshida-honmachi, Sakyo-ku, Kyoto 606-8501, Japan.

* Electrochemistry Society Active Member
[z]Corresponding Author:
E-mail Address: yasuda.kouji.3v@kyoto-u.ac.jp (K. Yasuda)

ORCID
Kouji Yasuda: https://orcid.org/0000-0001-5656-5359
Rika Hagiwara: https://orcid.org/0000-0002-7234-3980

Abstract

A novel process for the recycling of tungsten from hard tool scraps using carbonate molten salts is proposed. As a fundamental study, the oxidative dissolution of tungsten metal into molten Na_2CO_3 under Ar–O_2 and Ar–O_2–CO_2 atmospheres was investigated at 1173 K. The results of the oxidative dissolution experiments and the detection of CO gas evolution by infrared spectroscopy revealed the existence of multiple oxidation mechanisms by peroxide/superoxide ions and carbonate ions. The feasibility of each oxidant was discussed by calculating potential–p_{CO_2} diagrams in molten Na_2CO_3 at 1173 K. The relationship between the potential and the reaction was investigated using cyclic voltammetry and potential–p_{CO_2} diagrams.

Keywords

Tungsten, Molten salts, Carbonate, Recycling

Introduction

Tungsten is one of the critical metals that demonstrates favorable properties such as high hardness, wear resistance, and thermal resistance. Tungsten is processed into special steel (e.g., high-speed steel and heat-resistant steel, cemented hard tools (e.g., cutting tools and abrasive tools), and processed materials (e.g., plates, wires, and bars) for lighting and electronic components. Cemented hard tools are composed of tungsten carbide (WC) particles and cobalt metal binders. The application includes a wide range of industrial fields such as automobiles, aircrafts, and civil engineering. In 2017, the application of cemented hard tools accounted for approximately 80% in Japan.[1]

China dominates the supply of the tungsten resource with *ca*. 60% reserves and 80% mine production.[2] In certain circumstances like mine accidents, the resource supply could be unstable. Consequently, it is important to ensure the resource security and recycle tungsten scraps to use as secondary resources. However, the domestic recycling rate in Japan was only 11.6% in 2017.[1] Thus, the recycling of the cemented hard tool scraps is urgently required.

There are three major recycling methods for cemented hard tool scraps that are commercially used globally: zinc alloying method, thermal oxidation method, and molten nitrate method.[3] In the zinc alloying method, WC particles are recovered by crashing the scraps after the alloying/dealloying reaction of metallic Zn and Co. In the thermal oxidation method, scraps are calcined in air at high temperature; then, the surface oxide layer is leached in the alkali solutions, which is a treatment called peeling. Since oxidation is limited to the surface layer, the necessity of repeated calcination and leaching is a drawback owing to the high process cost. In the molten nitrate method, which is the most modern method, the scraps are oxidatively dissolved in molten $NaNO_3$ at 700–900 °C using the oxidizing power of nitrate.[3–5] The resultant Na_2WO_4 is then purified by wet processing. Even though the fast reaction rate is an advantage, this method has several disadvantages due to the emission of NOx gas and the difficulty in controlling the intensive exothermic reaction. Other molten salt methods using sulfates or hydroxides have been reported as recycling processes for tungsten materials.[6–15]

This study proposes a novel molten carbonate method for recycling tungsten from cemented hard tool scraps. Figure 1 depicts a flowchart of the molten carbonate method. The scraps are oxidatively dissolved in molten Na_2CO_3 under an $Ar–O_2–CO_2$ atmosphere. The produced Na_2WO_4 is treated using the same wet processing and hydrogen reduction of WO_3 as the molten nitrate method. Single Na_2CO_3 was chosen from various single and mixed carbonates because it allows the use of solid-liquid separation and ion exchange in the downstream process for sodium systems, which have been already established in industrial scale for the molten nitrate method.[3–5] One of the advantages of this method is that it does not require repeated peeling since the use of molten carbonate enables the

dissolution of the formed oxide into the molten salt. Another advantage is its environmentally friendliness due to the avoidance of NOx gas emissions. In addition, the reaction is easily controlled by the partial pressures of O_2 and CO_2, which are the parameters for oxidation and basicity, respectively. However, a disadvantage is that the reaction speed of the oxidation reaction for the proposed method is slower than that for the molten nitrate method.

Since oxidative dissolution reaction is a corrosion reaction, several methods were used to analyze the corrosion of metals in molten carbonates. The corrosion behavior in molten Li_2CO_3–K_2CO_3 was investigated for application in molten carbonate fuel cells (MCFC), and analyzed for Fe, Ni, Cr, and stainless steel using thermogravimetry[16–21] and for Ni, Fe–Cr alloy, and Ni–Fe alloy using electrochemical methods.[22–25] The oxidation and corrosion of these metals occur by peroxide (O_2^{2-}) and superoxide (O_2^-) ions formed by the chemical dissolution of O_2 gas into the melt.[26]

$$2CO_3^{2-}\,(l) + O_2\,(g) \rightarrow 2CO_2\,(g) + 2O_2^{2-}\,(l) \quad [1]$$

$$n O_2^{2-}\,(l) + 2M\,(s) \rightarrow 2M^{n+}\,(l) + 2nO^{2-}\,(l) \quad [2]$$

$$2CO_3^{2-}\,(l) + 3O_2\,(g) \rightarrow 2CO_2\,(g) + 4O_2^{-}\,(l) \quad [3]$$

$$2n O_2^{-}\,(l) + 2M\,(s) \rightarrow 2M^{n+}\,(l) + 2nO^{2-}\,(l) \quad [4]$$

However, the corrosion behavior of less common metals including tungsten in molten carbonates is scarce, and the reaction of W metal and WC to molten carbonates is only reported in vacuum at 1123 K[27] and in air at 1073–1273 K.[28] These reports only demonstrated the products without any analytical results for the reaction mechanism. In particular, the dependence on partial pressure of CO_2, which is the controlling factor for the basicity of molten carbonates, has not been investigated.

Since the elucidation of the reaction mechanism is crucial to achieve the proposed recycling process, this study was aimed at providing a knowledge on the thermodynamics and kinetics of the oxidative dissolution of cemented hard tools into molten Na_2CO_3 by selecting W metal as the model sample. First, the quantity of W metal oxidatively dissolved in molten Na_2CO_3 under an Ar–O_2–CO_2 atmosphere at 1173 K was measured, and the reaction mechanism was discussed using the dependence on CO_2 partial pressure, reaction in an Ar–CO_2 atmosphere, and gas analysis. Second, the oxidative dissolution of W metal and WC was analyzed using thermodynamic calculations. Last, several factors of oxidative dissolution such as oxidant species and corrosion potential were investigated cyclic voltammetry.

*** Fig. 1 ***

Experimental

Oxidative dissolution in Na_2CO_3 molten salt.

Figure 2 illustrates the experimental setup used for the oxidative dissolution experiment. Powdery Na_2CO_3 (Fuji Film Wako Pure Chemical Corp., >99.8%) and W plate (Nilaco Corp., 99.95%, *ca*. 10 × 10 × 0.3 mm) were placed in an alumina crucible (Nikkato Corp., SSA-S, C1, 30 mL, height 24 mm) and dried overnight in a vacuum at 453 K. The Na_2CO_3 powder was weighed such that the depth of molten salt was 4 mm, 6 mm, or 9 mm. The three crucibles with melts at different depths were set on an Au base plate (Nilaco Corp., thickness 0.1 mm) to prevent the upset and tilting, and were inserted into an airtight vessel composed of a stainless-steel flange and a quartz reaction tube (outer diameter: 46 mm, inner diameter: 42 mm, length: 400 mm). The temperature of the reaction tube set in a horizontal furnace was raised from room temperature to 1173 K at a rate of 5 K min^{-1} and maintained for a reaction time of 0–2.5 h, where the melting temperature of Na_2CO_3 is 1131 K. After the reaction, the temperature was lowered to room temperature at a rate of 5 K min^{-1}. Herein, the reaction time indicates the duration for which the furnace was maintained at 1173 K. Thus, at 0 h, the reaction was conducted only by raising the temperature to 1173 K then immediately lowering the temperature without holding at that temperature. The flow rate of the mixed-gas was controlled by a mass flow controller (Horiba STEC Co. Ltd., SEC-E40 or PE-D20). The flow rate was fixed to 50 mL min^{-1} and the partial pressure was controlled by each flow rate; the partial pressure of CO_2 at 6×10^{-4} atm was attained at a rate of 0.03 mL min^{-1}. The flowing gas was Ar–CO_2 (6×10^{-4}–0.8 atm) during the heating and cooling, then switched to Ar–O_2–CO_2 (Ar–O_2: 0.2 atm, CO_2: 6×10^{-4}–0.8 atm) during the reaction at 1173 K. The partial pressure of CO_2 was kept constant throughout the experiment. In the experiment used to investigate the reaction mechanism without the effect of O_2 gas, the reaction was conducted in Ar–CO_2 (6×10^{-4}–0.8 atm). In several experiments, the outlet gas from the furnace was sampled into a plastic bag and analyzed using Fourier transform infrared spectroscopy (FT-IR, Bruker Corp., ALPHA II).

The recovered salts were crushed in a mortar and analyzed by X-ray diffraction (XRD, Rigaku Corp., MiniFlex, Cu-*Kα* line, 30 kV, 10 mA). The weight change in the W plate and the amount of W dissolved in the molten carbonate determined by inductive coupled plasma-atomic emission spectroscopy (ICP-AES, Hitachi Ltd., SPECTRO BLUE) correlated with each other. The dissolved thickness of the W plate (x_w) was evaluated from the weight of the plate before the reaction ($w_{W,bef}$)

and the weight loss ($w_{W,dec}$). The evaluation was made under the assumption that the dissolution reaction only proceeded from the upper surface of the plate.

$$x_w\,(\mu m) = 300 \times w_{W,dec} / w_{W,bef} \quad [5]$$

*** Fig. 2 ***

Electrochemical analysis in the Na_2CO_3 molten salt.

Fig. 3 depicts a schematic drawing of the experimental apparatus used in electrochemical measurements. Na_2CO_3 (300 g) was charged in an alumina crucible (As One Corp., >99%, outer diameter: 90 mm, inner diameter: 80 mm, height: 140 mm) and dried under vacuum at 453 K for more than 12 h to remove the moisture. The crucible was then placed at the bottom of a quartz vessel in an airtight quartz container in a vertical furnace. The controlled atmosphere was as described above. The measurement was conducted in Ar–O_2–CO_2 (Ar–O_2: 0.2 atm, CO_2: 6×10^{-4} atm) and Ar–O_2–CO_2 (Ar–O_2: 0.2 atm, CO_2: 0.8 atm), hereinafter low-CO_2 and high-CO_2 partial pressures, respectively.

Electrochemical measurements were performed at 1173 K by a three-electrode method using an electrochemical measurement system (Hokuto Denko Corp., HZ-7000). The working electrodes were Au wire (Japan Metal Service, Ltd., 99.99%, diameter: 0.5 mm) and W plate (Nilaco Corp., 10 × 10 × 0.1 mm, 99.95%). Au plate (Japan Metal Service, Ltd., 99.99%, 0.1 mm thick) was used as a counter electrode. Au wire immersed in the molten salt was used as a quasi-reference electrode. Since the atmosphere and the molten salt contains O_2 gas and O^{2-} ions, respectively, the potential of the quasi-reference electrode would correspond to the O_2/O^{2-} equilibrium at the given partial pressure of O_2 gas and the activity of O^{2-} ions determined by the partial pressure of CO_2.

$$O_2\,(g) + 4e^- = 2O^{2-}\,(l) \quad [6]$$

$$CO_3^{2-}\,(l) = CO_2\,(g) + O^{2-}\,(l) \quad [7]$$

The potential of the quasi-reference electrode is discussed in results and discussion.

*** Fig. 3 ***

Results and Discussion

Oxidative dissolution and thermodynamic analysis.

After the reaction, white salt and W plate were recovered as shown in the photographs in Fig. 4(a) and (b), respectively, which were the representative reacted samples obtained under the conditions of 0.2 atm O_2, 6×10^{-4} atm CO_2, and 2.5 h. As shown in the XRD spectrum of the salt in Fig. 4(c), the diffraction peaks of Na_2WO_4 and Na_2CO_3 are confirmed, thus verifying the oxidative dissolution of the W plate as the W(VI) compound. The appearances and XRD patterns of the sample after the reaction were similar in all experimental conditions, despite changing the CO_2 partial pressure and reaction time.

*** Fig. 4 ***

Fig. 5 shows the dissolved thickness of the W plate in molten Na_2CO_3 at 1173 K under the Ar–O_2–CO_2 (Ar–O_2: 0.2 atm, CO_2: 6×10^{-4} atm) atmosphere against the reaction time for each melt depth. The dissolved thickness is larger at smaller melt depths. The dissolution rate determined from the slope between the reaction time of 0 and 2.5 h is 23.1, 9.8, and 6.8 μm h^{-1} at 4, 6, and 9 mm of the melt depth, respectively. The dependency of the reaction rate on the depth of the melt suggests that the rate determining step of the reaction is the diffusion between the gas-liquid interface at the melt surface and the solid-liquid interface at the surface of the W plate.

The corrosion and oxidative dissolution of the metals in molten carbonates are generally associated with four elementary steps.[26] Based on the reported mechanisms, the oxidative dissolution of W metal in this study consists of the following steps:

(1) Formation of O_2^{2-}/O_2^- ions by the chemical dissolution of O_2 gas at the gas-liquid interface

$2CO_3^{2-}(l) + O_2(g) \rightarrow 2CO_2(g) + 2O_2^{2-}(l)$ [1]

$2CO_3^{2-}(l) + 3O_2(g) \rightarrow 2CO_2(g) + 4O_2^{-}(l)$ [3]

(2) Diffusion of O_2^{2-}/O_2^- ions from the gas-liquid interface to the solid-liquid interface

O_2^{2-} (l, gas/liquid) $\rightarrow$ O_2^{2-} (l, liquid/solid) [8]

O_2^{-} (l, gas/liquid) $\rightarrow$ O_2^{-} (l, liquid/solid) [9]

(3) Formation of WO_4^{2-} ions by the oxidation of W metal

$W(s) + 3O_2^{2-}(l) \rightarrow WO_4^{2-}(l) + 2O^{2-}(l)$ [10]

$W\ (s) + 2O_2^-\ (l) \rightarrow WO_4^{2-}\ (l)$ [11]

(4) Diffusion of WO_4^{2-} ions from the solid-liquid interface to the bulk melt

$WO_4^{2-}\ (l, \text{liquid/solid}) \rightarrow WO_4^{2-}\ (l, \text{bulk})$ [12]

The existence of O_2^{2-}/O_2^- ions at high partial pressure of CO_2 has been intensively reported in MCFC researches.[29–42] Their high stability at low partial pressure was also experimentally confirmed.[43,44] According to the report by Andersen,[43] when the O_2–O_2^-–O_2^{2-}–O^{2-} equilibria were attained for various carbonate molten salts of Li, Na, and/or K by holding in O_2 (1 atm) after adding 3 mol% O^{2-} ions, a large amount of the added O^{2-} ions reacted with O_2 gas to form O_2^{2-}/O_2^- ions at the low partial pressure of CO_2 (the estimated order of 10^{-4} or 10^{-3} atm) by the formed gas in CO_3^{2-} dissociation. Of these four elementary steps, steps (2) and (4) correspond to diffusion. Here, the diffusion rate for the WO_4^{2-} ions in (4) is determined by the thickness of diffusion layer rather than by the melt depth. In addition, the solubility of the WO_4^{2-} ions is very high as the Na_2CO_3–$Na_2W_2O_7$ system shows liquid state for the entire composition at 1173 K.[45] Therefore, the diffusion of O_2^{2-} and O_2^- ions from the gas-liquid to the solid-liquid interface (step (2)) is the rate-determining step. The dissolution reaction at (3) is fast enough to keep the ion concentration at the surface of the W plate constant, and the rapid reaction rate is attained by a higher concentration gradient at a smaller melt depth and a diffusion distance of O_2^{2-}/O_2^- oxidants.

In Fig. 5, the dissolution of the reaction at 0 h for each melt depth occurs at *ca*. 10 μm. Since O_2 gas was not supplied during the reaction at 0 h, this dissolution occurs in another oxidation mechanism except in the case of O_2^{2-}/O_2^- oxidants. The most probable oxidants are CO_3^{2-} ions at this stage.

*** Fig. 5 ***

The confirmation that CO_3^{2-} ions also function as oxidants was carried by three types of the oxidative dissolution experiment in the Ar–CO_2 atmosphere without O_2 gas to observe the characteristic of CO_3^{2-} oxidants. First is the occurrence of dissolution without O_2 gas. The appearance and XRD pattern of the recovered salt and W plate after the reaction were similar regardless the existence of O_2 gas. The dissolved thickness of the W plate at the 6-mm melt depth for 2.5 h at each CO_2 partial pressure is shown in Fig. 6(a), and a dissolved thickness of approximately 25 μm is observed even without O_2^{2-}/O_2^- oxidants. Second is an oxidative dissolution at different melt depths in the Ar–CO_2 (0.8 atm) atmosphere. The circle and triangle in Fig. 6(a) show the dissolved thickness

for 6 and 9 mm of the melt depth, respectively. The identical dissolved thickness agrees with the characteristic of the CO_3^{2-} ions that they exist abundantly in the neighboring region of the molten salt/W plate interface, which do not require diffusion from the gas/liquid interface. Third experiment involved IR spectroscopy of the outlet gas. The IR measurement was conducted only for the oxidative dissolution experiment in the Ar–CO_2 atmosphere without O_2 gas so that the combustion of CO gas by the O_2 component gas to form CO_2 gas should be avoided. Fig. 6(b) shows the IR spectrum of the exhaust gas for the oxidative dissolution experiment of tungsten under Ar–CO_2 (0.2 atm) atmosphere in molten Na_2CO_3 at 1173 K. In addition to the component CO_2 gas, a sharp peak ascribed to the CO gas is detected which is the byproduct of CO_3^{2-} oxidants. These three experiments clearly confirmed that the CO_3^{2-} ions function as an oxidant for the W metal. The representative reaction is as follows:

$$CO_3^{2-}\,(l) + 2e^- \rightarrow 2O^{2-}\,(l) + CO\,(g) \qquad [13]$$

$$W\,(s) + 3CO_3^{2-}\,(l) \rightarrow WO_4^{2-}\,(l) + 2O^{2-}\,(l) + 3CO\,(g) \qquad [14]$$

Studies on corrosion protection for MCFC applications have confirmed that the oxidation responsible for metal corrosion in molten carbonate occurs by O_2^{2-}/O_2^- ions.[26] Here, it should be noted that this study confirmed that CO_3^{2-} ions also function as oxidants.

*** Fig. 6 ***

Since the oxidizing ability of CO_3^{2-} ions was experimentally verified, its thermodynamic aspect was investigated by drawing a potential–p_{CO_2} diagram by referring to a previous report by Cassir *et al.*[46] where p_{CO_2} is the partial pressure of CO_2 gas. The diagram draws the equilibrium conditions and stable region of the related species, where the electrode potential and logarithm of partial pressure of CO_2 were the vertical and horizontal axes, respectively.[47] The standard Gibbs energy of formation (ΔG°_f) for the compounds at 1173 K used for the potential–p_{CO_2} diagram is summarized in Table 1.[48,49] The standard Gibbs energy of formation of ionic species are defined by selecting the standard ion and standard potential as follows: the O^{2-} (l) ion is selected as the standard ion and its standard state is the virtual state of the pure Na_2O (l) in Na_2CO_3 (l). The standard potential is settled for the equilibrium potential for O_2 (g, 1 atm)/O^{2-} (l, a = 1).

O_2 (g) + 4e$^-$ = 2O^{2-} (l) [6]

The standard Gibbs energy of formation of ionic species at 1173 K determined by the above definition is listed in Table 2.[48,49] Here, the values for O_2^{2-} (l) and O_2^- (l) were calculated under the assumption that the reported molar fraction of O^{2-}:O_2^{2-}:0.5O_2^- = 51:39:10 mol% at 1200 K remains applicable at 1173 K; the aforementioned values were attained at the equilibrium with O_2 (1 atm) gas after adding 3 mol% O^{2-} ions to the molten Na_2CO_3.[43]

The potential–p_{CO_2} diagram for the molten Na_2CO_3 at 1173 K, which was calculated from the reported thermodynamic data, is shown in Fig. 7. The region enclosed by the blue lines corresponds to the stable region of the molten Na_2CO_3. The following reactions determine the various limits:

(1) Precipitation of Na_2O (s)

Na_2CO_3 (l) = Na_2O (s) + CO_2 (g) [15]

$\log p_{CO_2} = -7.11$ [16]

(2) Evolution of O_2 gas (anodic limit)

O_2 (g, 1 atm) + 4e$^-$ = 2O^{2-} (l) [17]

$E = 0.116 \log p_{CO_2} + 0.870$ (V) [18]

(3) Evolution of Na gas (cathodic limit)

Na^+ (l) + e$^-$ = Na (g) [19]

$E = -1.273$ (V) [20]

(4) Evolution of CO gas (cathodic limit)

CO_3^{2-} (l) + 2e$^-$ = 2O^{2-} (l) + CO (g) [21]

$E = 0.233 \log p_{CO_2} - 0.116 \log p_{CO} - 0.066$ (V) [22]

(5) Deposition of carbon (cathodic limit)

CO_3^{2-} (l) + 4e$^-$ = 3O^{2-} (l) + C (s) [23]

$E = 0.175 \log p_{CO_2} - 0.156$ (V) [24]

(6) Formation of O_2^{2-} ions

O_2^{2-} (l) + 2e$^-$ = 2O^{2-} (l) [25]

$E = 0.233 \log p_{CO_2} + 0.116 \log a_{O_2^{2-}} - 1.754$ (V) [26]

(7) Formation of O_2^- ions

O_2^- (l) + 3e$^-$ = 2O^{2-} (l) [27]

$E = 0.155 \log p_{CO_2} + 0.078 \log a_{O_2^-} + 1.262$ (V) [28]

where, E is the potential, p_{CO} is the partial pressure of CO gas, and $a_{O_2^{2-}}$ and $a_{O_2^-}$ are the activities of O_2^{2-} and O_2^- ions, respectively.

The oxidation power of the two oxidants, O_2^{2-}/O_2^- ions and CO_3^{2-} ions, in the molten Na_2CO_3 is depicted in the diagram. The positive redox potentials for reactions (6) and (7) indicate that the O_2^{2-}/O_2^- ions exhibit strong oxidation power. Thus, the O_2^{2-}/O_2^- ions function as oxidants, even for a species with relatively positive corrosion potential. On the other hand, the oxidation power of the CO_3^{2-} ions in reactions (4) and (5) is so weak that only species with more negative corrosion potentials than those of the CO_3^{2-}/CO and CO_3^{2-}/C equilibriums are oxidized. In other words, both the CO_3^{2-} and O_2^{2-}/O_2^- ions function as oxidants for that kind of negative species. The solubility of the CO gas physically dissolved into molten carbonates is in the order of 10^{-7} mol cm^{-3} atm^{-1}.[50,51] The solubility of the chemical dissolution to form CO_2^{2-} ions is larger, in the order of 10^{-6} mol cm^{-3} atm^{-1}.[50,51]

$$CO + O^{2-} = CO_2^{2-} \quad [29]$$

$$CO + CO_3^{2-} = CO_2^{2-} + CO_2 \quad [30]$$

The broken lines in Fig. 7 show that the product of the CO_3^{2-} oxidant varies with the partial pressure of CO. When the corrosion potential is substantially negative, the product could be CO gas bubble at 1 atm pressure. At more positive potentials, the partial pressure of CO is lower and the product is either physically dissolved CO gas or chemically dissolved CO_2^{2-} ions.

The potential–p_{CO_2} diagram for the W species in molten Na_2CO_3 at 1173 K is also drawn in Fig. 7 with red and orange lines for W and WC, respectively. The corresponding reactions and conditions are shown below. The precipitation of solid WO_3 is depicted on the far right outside the frame of the figure.

(8) Equilibrium of WO_4^{2-}/W

$$WO_4^{2-}\,(l) + 6e^- = W\,(s) + 4O^{2-}\,(l) \quad [31]$$

$$\boldsymbol{E = 0.155 \log p_{CO_2} + 0.039 \log a_{WO_4^{2-}} - 0.332} \quad \text{(V)} \quad [32]$$

(9) Equilibrium of WO_4^{2-}/WO_3

$$WO_3\,(s) + O^{2-}\,(l) = WO_4^{2-}\,(l) \quad [33]$$

$$\boldsymbol{\log p_{CO_2} = -\log a_{WO_4^{2-}} + 6.786} \quad [34]$$

(10) Equilibrium of WO_3/W

$$WO_3\,(l) + 6e^- = W\,(s) + 3O^{2-}\,(l) \quad [35]$$

$$E = 0.116 \log p_{CO_2} - 0.069 \quad \text{(V)} \qquad [36]$$

(11) Equilibrium of WO_4^{2-}/WC

$$WO_4^{2-}\,(l) + CO_2\,(g) + 10e^- = WC\,(s) + 6O^{2-}\,(l) \qquad [37]$$

$$E = 0.163 \log p_{CO_2} + 0.023 \log a_{WO_4^{2-}} - 0.225 \quad \text{(V)} \qquad [38]$$

(12) Equilibrium of WO_3/WC

$$WO_3\,(l) + CO_2\,(g) + 10e^- = WC\,(s) + 5O^{2-}\,(l) \qquad [39]$$

$$E = 0.140 \log p_{CO_2} - 0.067 \quad \text{(V)} \qquad [40]$$

The red and orange lines indicate the WO_4^{2-}/W and WO_4^{2-}/WC equilibriums for an activity of WO_4^{2-} ions ($a_{WO_4^{2-}}$) of 10^{-2} locate at more negative than the thermodynamic stable region of molten Na_2CO_3 at all CO_2 partial pressures, respectively. These redox potentials clearly indicate that the oxidation of W and WC by CO_3^{2-} ions, which was experimentally confirmed in Fig. 6, is thermodynamically favorable. Therefore, these results verify that the oxidative dissolution of W metal in molten Na_2CO_3 proceeds with both O_2^{2-}/O_2^- and CO_3^{2-} ions as oxidants (Fig. 8). One mechanism is (a) oxidation by O_2^{2-}/O_2^- ions produced by the chemical dissolution of O_2 gas into the molten salt.

$$W\,(s) + 3O_2^{2-}\,(l) \rightarrow WO_4^{2-}\,(l) + 2O^{2-}\,(l) \qquad [10]$$

$$W\,(s) + 2O_2^{-}\,(l) \rightarrow WO_4^{2-}\,(l) \qquad [11]$$

The other mechanism is (b) oxidation by CO_3^{2-} ions.

$$W\,(s) + 3CO_3^{2-}\,(l) \rightarrow WO_4^{2-}\,(l) + 2O^{2-}\,(l) + 3CO\,(g) \qquad [14]$$

*** Table 1 ***

*** Table 2 ***

*** Fig. 7 ***

*** Fig. 8 ***

The dependence of the dissolved thickness of the W plates on the partial pressure of CO_2 for the molten Na_2CO_3 at 1173 K under the Ar–O_2–CO_2 atmosphere (Ar–O_2: 0.2 atm) for 2.5 h is shown in Fig. 9. Although there is a negative correlation between the dissolved thickness and CO_2 partial

pressure at low-CO_2 partial pressures, there is a positive correlation at high-CO_2 partial pressures. The dependence at low-CO_2 partial pressures occurs by the strong influence of oxidation by O_2^{2-}/O_2^- ions. The chemical dissolution of O_2 gas into molten Na_2CO_3 in reactions [1] and [3] is suppressed by the increase in CO_2 partial pressure. Then, the lowered diffusion flux of O_2^{2-}/O_2^- ions results in a smaller dissolved thickness of the W plate. On the other hand, the positive correlation in the high-CO_2 region is due to the oxidation by CO_3^{2-} ions, which is facilitated by the low activity of O^{2-} ions at high-CO_2 partial pressures (reaction [14]).

*** Fig. 9 ***

Cyclic voltammetry.

The electrochemistry of molten Na_2CO_3 was investigated by cyclic voltammetry at 1173 K. The voltammogram at low-CO_2 partial pressure, Ar–O_2–CO_2 (Ar–O_2: 0.2 atm, CO_2: 6×10^{-4} atm), was measured using an Au electrode and is shown in Fig. 10(a). The rest potential is 0 V vs. Au because the working and quasi-reference electrodes were both made of Au immersed in the molten salt. In the potential sweep to the negative direction, a small reduction current is observed from the rest potential, then a large reduction current starts at approximately −0.85 V. The reduction current sharply increases at −1.7 V. After the reversal of the sweep direction, the oxidation current starts to flow at 0 V and has a peak at 0.7 V. The potential of the quasi-reference electrode can be calibrated to the value indicated in the potential– $\boldsymbol{p_{CO_2}}$ diagram (Fig. 7) under the conditions that the O_2/O^{2-} reaction is electrochemically reversible and the potential of the reference electrode corresponds to the O_2/O^{2-} equilibrium at the given partial pressure.

$O_2\,(g) + 4e^- = 2O^{2-}\,(l)$ [41]

$$\boldsymbol{E = 0.116 \log p_{CO_2} + 0.058 \log p_{O_2} + 0.870} \quad \text{(V)} \qquad [42]$$

Because the estimated equilibrium potential of the Au quasi-reference electrode is 0.455 V (vs. O_2 (1 atm)/O^{2-} (a = 1)) at $\boldsymbol{p_{CO_2}}$ = 6×10^{-4} atm and $\boldsymbol{p_{O_2}}$ = 0.2 atm, the calibration enables analysis of the cyclic voltammogram. Here, the calibration assumption should be noticed that the reversibility for electrochemical reaction [41] is unknown for low partial pressure of CO_2 although it is well-known for high partial pressure and the utilization of an Au electrode in 67%CO_2–33%O_2 gas as a reference

electrode has been established. The oxidation at potentials more positive than 0 V indicates the evolution of O_2 gas. The small reduction current from 0 V to −0.8 V indicates the reduction of O_2 gas. The large reduction current at −0.85 V corresponds to $\boldsymbol{p_{CO}} = 10^{-3}$ atm for the reduction of CO_3^{2-} ions (reaction [21]). At this potential, CO_2^{2-} ions are produced because the partial pressure of CO is too small for it to be gas bubbles. The large reduction current at −1.7 V corresponds to the evolution potential of Na gas (reaction [19] and equation [20]). In summary, the reactions in molten Na_2CO_3 at low-CO_2 partial pressure and at 1173 K are identified as shown by the arrows at the bottom in Fig. 10(a): (A) O_2 gas evolution at potentials more positive than 0 V, (B) O_2 reduction at potentials more negative than 0 V, (C) CO_3^{2-} reduction to CO_2^{2-} ions, and (D) Na gas evolution. While the strict agreement of the potential for (D) Na gas evolution at −1.7 V suggests the validity of the calibration or the error within the range of 0.05 V, the reversibility of O_2/O^{2-} redox reaction on an Au electrode should be investigated in the future. At this CO_2 partial pressure, the rest potential, i.e. the corrosion potential, of the W metal electrode is −0.94 V vs. Au. This potential clearly indicates that the oxidant of the W metal is not only O_2^{2-}/O_2^- ions but also CO_3^{2-} ions because it is in the potential region of (C) CO_3^{2-} reduction to CO_2^{2-} ions.

Cyclic voltammetry was also conducted at high-CO_2 partial pressure, O_2–CO_2 (O_2: 0.2, CO_2: 0.8 atm). The voltammogram obtained on an Au electrode is indicated in Fig. 10(b). Although the small reduction current of approximately –10 mA cm^{-2} starting at 0 V is the same as that at low-CO_2 pressure, the increase in the reduction current at −1.2 V is smaller. A small anodic current peak is observed after the reversal at −1.8 V. Since the equilibrium potential of O_2/O^{2-} at the given atmosphere is 0.818 V (vs. O_2 (1 atm)/O^{2-} (a = 1)), the potential region and corresponding reaction are analyzed as follows: (A) O_2 gas evolution at potentials more positive than 0 V, (B) O_2 reduction at potentials more negative than 0 V, (C) CO_3^{2-} reduction to CO_2^{2-} ions at $E < -0.6$ V, and (E) CO_3^{2-} reduction to C deposition at $E < -0.9$ V. The existence of an overpotential for the C deposition on the Au electrode is suggested since the starting potential is more negative than that by the thermodynamic estimation. The rest and corrosion potential of W metal of −1.20 V at high-CO_2 pressure are in the potential region of (E) CO_3^{2-} reduction to C deposition, and both the O_2^{2-}/O_2^- and CO_3^{2-} ions thermodynamically function as the oxidants of the W metal.

*** Fig. 10 ***

Characteristics of O_2^{2-}/O_2^- and CO_3^{2-} oxidants.

As explained in Fig. 8, the oxidative dissolution of the W metal into molten Na_2CO_3 proceeds in two mechanisms. The comparison of the dissolved thickness of the W metal in Ar–O_2–CO_2 (Fig. 9) and Ar–CO_2 (Fig. 6(a)) atmospheres shows that the contribution of O_2^{2-}/O_2^- ions is almost comparable with that of CO_3^{2-} ions despite the strong oxidizing power, as indicated by the positive redox potential in the potential–$\boldsymbol{p_{CO_2}}$ diagram. The reason for the aforementioned observation is the solubility in molten Na_2CO_3. The solubility of the O_2^{2-}/O_2^- ions at 0.2 atm O_2 partial pressure calculated from the report by Appleby and Drunen[50] is in the order of 10^{-7} mol cm^{-3}. On the other hand, the concentration of CO_3^{2-} ions calculated from the density of Na_2CO_3 (1.953 g cm^{-3} at 1173 K)[52] is 1.84×10^{-2} mol cm^{-3}. A concentration value that is five orders of magnitude is the source of the relatively large contribution of CO_3^{2-} ions despite the small oxidation power.

Among the oxidants, an enhanced dissolution rate is expected for the oxidation by O_2^{2-}/O_2^- ions. The increase in the dissolution rate by CO_3^{2-} oxidants is probably difficult because the concentration of CO_3^{2-} ions in the melt is constant and the rate is independent of CO_2 partial pressure, as shown in Fig. 6(a). The increase in the dissolution rate by the O_2^{2-}/O_2^- oxidant is expected to be possible because it depends on the melt depth, CO_2 partial pressure, and concentration of O_2^{2-}/O_2^- ions. The typical improvement is the introduction of O_2 gas into the molten salt to shorten the diffusion distance of the O_2^{2-}/O_2^- ions to the scrap surface.

Conclusions

The molten carbonate method was proposed as a new recycling process of tungsten contained in cemented hard tools. As a fundamental study of this process, W metal was selected as the model sample, and the thermodynamics and kinetics for the oxidative dissolution of W metal into molten Na_2CO_3 at 1173 K were investigated. Oxidative dissolution and the formation of Na_2WO_4 were confirmed in the Ar–O_2–CO_2 atmosphere at various partial pressures of CO_2. The dissolution rate in the Ar–O_2–CO_2 atmosphere was dependent on the CO_2 partial pressure by changing the basicity. The dissolution of W metal was also confirmed in the Ar–CO_2 atmosphere without O_2 gas, which confirmed the ability of CO_3^{2-} ions to behaved as an oxidant for W metal, as supported by thermodynamics using the calculated potential–p_{CO_2} diagram. The results obtained in this study verified that the oxidative dissolution of W metal into molten Na_2CO_3 proceeds via two types of oxidation mechanisms by O_2^{2-}/O_2^- ions and CO_3^{2-} ions.

Acknowledgments

This study was partly supported by Tokyo Ohka Foundation for the Promotion of Science and Technology, Japan Oil, Gas and Metals National Corporation (JOGMEC), and Kyoto Education Foundation for the Promotion of Science and Technology. The authors thank to Prof. T. Nohira at Institute of Advanced Energy of Kyoto University for ICP-AES measurements.

References

1. JOGMEC, *Material Flow of Mineral Resources 2018*, 13. Tungsten (2019).
2. U.S. Geological Survey, *Mineral Commodity Summaries 2020* (2020).
3. Y. Yamamoto, K. Sasaya, T. Fudo, A. Nakano, S. Yamanaka, T. Iguchi, F. Sato, and A. Ikegaya, PCT International Patent, WO2010/104009 (2010).
4. T. Ishida, T. Itakura, H. Moriguchi, and A. Ikegawa, *SEI Technical Review*, **181**, 33 (2012).
5. T. Hayashi, F. Sato, K. Sasaya, and A. Ikegaya, *SEI Technical Review*, **189**, 8 (2016).
6. F. H. Scott, United Kingdom Patent, GB791925 (1955).
7. R. Simon, German Patent, DE3144295 (1981).
8. A. D. Douglass, K. T. Reilly, and J. E. Landmesser, US Patent, US4603043 (1986).
9. S. N. Bhosale, S. Mookherjee, and R. M. Pardeshi, *High. Temp. Mater. Processes*, **9**, 147 (1990).
10. E. Lassner, *Int. J. Refract. Met. Hard Mater.*, **13**, 35 (1995).
11. M. Lohse, PCT International Patent, WO96/041768 (1996).
12. K. B. Shedd, Tungsten Recycling in the United States in 2000, U.S. Geological Survey (2005).
13. M. Morishita, H. Yamamoto, M. Ikebe, H. Yanagida, and T. Ueno, PCT International Patent, WO2014/045579 (2014).
14. T. Itakura, A. Ikegaya, and Y. Yamamoto, Japanese Patent, 6018958 (2016).
15. T. Oishi, *Kinzoku*, **87**, 771 (2017).
16. K. N. Lee and D. A. Shores, *J. Electrochem. Soc.*, **137**, 859 (1990).
17. B. Kim, H. Yoshitake, H. Yokokawa, N. Kamiya, and K. Ota, *Bull. Chem. Soc. Jpn*., **66**, 1366 (1993).
18. B. Kim, H. Yoshitake, N. Kamiya, and K. Ota, in *Proc. Int. Symp. Molten Salt Chemistry and Technology*, M. L. Saboungi and H. Kojima, Editor, PV 93-9, p.321, The Electrochemical Society Proceedings Series, Pennington, NJ (1993).
19. K. Ota, S. Mitsushima, K. Kato, and N. Kamiya, in *2nd Symp. Molten Carbonate Fuel Cell Technology*, J. R. Selman, D. A. Shores, H. C. Maru, and I. Uchida, Editors, PV 90-16, p.318, The Electrochemical Society Proceedings Series, Pennington, NJ (1990).
20. K. Ota, K. Toda, T. Kojima, N. Motohira, and N. Kamiya, in *Proc. 10th Int. Symp. Molten Salts*, R. T. Carlin, S. Deki, M. Matsunaga, D. S. Newman, J. R. Selman, and G. R. Stafford, Editors, PV 96-7, p.406, The Electrochemical Society Proceedings Series, Pennington, NJ (1996).
21. M. Yanagita, S. Baba, K. Takimoto, T. Kojima, N. Ohtori, Y. Tamiya, T. Asai, Y. Miyazaki, and M. Azuma, *Denki Kagaku (Electrochemistry)*, **64**, 445 (1996).

22. A. Nishikata and S. Haruyama, *Corrosion*, **42**, 528 (1986).
23. J. P. T. Vossen, L. Plomp, and J. H. W. de Wit, *J. Electrochem. Soc.*, **141**, 3040 (1994).
24. J. P. T. Vossen, A. H. H. Janssen, and J. H. W. de Wit, *J. Electrochem. Soc.*, **143**, 58 (1996).
25. H. Matsuyama, T. Nishina, and I. Uchida, in *Proc. Int. Symp. Molten Salt Chemistry and Technology*, M. L. Saboungi and H. Kojima, Editor, PV 93-9, p.436, The Electrochemical Society Proceedings Series, Pennington, NJ (1993).
26. Y. Ito, *Yoyuen no Kagaku*, Industrial Publishing & Consulting, Inc., Tokyo (2005).
27. M. C. Ball, D. S. Brown, D. Page, and R. R. T. Thurman, *Brit. Ceram. Trans. J.*, **66**, 307 (1967).
28. F. H. Scott, United Kingdom Patent, GB791925 (1955).
29. A. J. Appleby and S. Nicholson, *J. Electroanal. Chem. Interfacial Electrochem.*, **53**, 105 (1974).
30. A. J. Appleby and S. B. Nicholson, *J. Electroanal. Chem. Interfacial Electrochem.*, **83**, 309 (1977).
31. A. J. Appleby and S. B. Nicholson, *J. Electroanal. Chem. Interfacial Electrochem.*, **112**, 71 (1980).
32. G. B. Dunks and D. Stelman, *Inorg. Chem.*, **22**, 2168 (1983).
33. W. M. Vogel, S. W. Smith, and L. J. Bregoli, *J. Electrochem. Soc.*, **130**, 574 (1983).
34. I. Uchida, T. Nishina, Y. Mugikura, and K. Itaya, *J. Electroanal. Chem.*, **206**, 229 (1986).
35. I. Uchida, T. Nishina, Y. Mugikura, and K. Itaya, *J. Electroanal. Chem.*, **206**, 241 (1986).
36. I. Uchida, T. Nishina, Y. Mugikura, and K. Itaya, *J. Electroanal. Chem.*, **209**, 125 (1986).
37. S. H. Lu and J. R. Selman, *J. Electrochem. Soc.*, **137**, 1125 (1990).
38. G. L. Lee and J. R. Selman, *Electrochim. Acta*, **38**, 2281 (1993).
39. P. Tomczyk, H. Sato, K. Yamada, T. Nishina, and I. Uchida, *J. Electroanal. Chem.*, **391**, 125 (1995).
40. R. W. Reeve and A. C. C. Tseung, *J. Electroanal. Chem.*, **403**, 69 (1996).
41. M. Cassir, B. Malinowska, W. Peelen, K. Hemmes, and J. H. W. de Wit, *J. Electroanal. Chem.*, **433**, 195 (1997).
42. T. Itoh, K. Abe, K. Dokko, M. Mohamedi, I. Uchida, and A. Kasuya, *J. Electrochem. Soc.*, **151**, A2042 (2004).
43. B. K. Andersen, *Acta Chem. Scand.*, **A31**, 242 (1977).
44. G. Moutiers, M. Cassir, and J. Devynck, J. Electroanal. Chem. Interfacial Electrochem., 315, 103 (1991).
45. E. M. Levin, C. R. Robbins, and H. F. McMurdie, *Phase Diagrams for Ceramists 1969*

Supplement, The American Ceramic Society, Columbus, p. 82 (1969).

46. M. Cassir, G. Moutiers, and J. Devynck, *J. Electrochem. Soc.*, **140**, 3114 (1993).
47. M. D. Ingram and G. J. Janz, *Electrochim. Acta*, **10**, 783 (1965).
48. I. Barin, *Thermochemical Data of Pure Substances*, *3rd Edition*, VCH, Weinheim (1995).
49. M. W Chase, *NIST-JANAF Thermochemical Tables, 4th Edition*, American Chemical Society and American Institute of Physics for the National Bureau of Standards, New York (1998).
50. A. J. Appleby and C. V. Drunen, *J. Electrochem. Soc.*, **127**, 1655 (1980).
51. A. Borucka and A. J. Appleby, *J. Chem. Soc., Farad. Trans. 1: Physical Chemistry in Condensed Phases*, **73**, 1420 (1977).
52. A. T. Ward and G. J. Janz, *Electrochim. Acta*, **10**, 849 (1965).

Figure Captions

Fig. 1 Flowchart of molten carbonate method for recycling of tungsten proposed in this study.

Fig. 2 Schematic drawing of oxidative dissolution experiment of tungsten metal at 1173 K. (A) Stainless steel lid, (B) SiO_2 reaction tube, (C) alumina tube, (D) electric furnace, (E) alumina crucible, (F) molten Na_2CO_3, (G) W plate, and (H) Au plate.

Fig. 3 Schematic drawing of electrochemical measurement of tungsten metal at 1173 K. (A) Stainless steel lid, (B) SiO_2 reaction tube, (C) electric furnace, (D) alumina crucible, (E) molten Na_2CO_3, (F) W plate electrode, (G) Au wire electrode, and (H) Au plate electrode.

Fig. 4 Representative appearance of (a) the recovered salt and (b) W plate, and (c) XRD pattern of the salt after oxidative dissolution experiment of tungsten plate for 2.5 h in molten Na_2CO_3 with 6-mm melt depth at 1173 K in Ar–O_2(0.2 atm)–CO_2(6×10^{-4} atm) atmosphere.

Fig. 5 Dissolved thickness of tungsten plates in molten Na_2CO_3 at 1173 K in Ar–O_2(0.2 atm)–CO_2(6×10^{-4} atm) atmosphere.

Fig. 6 (a) Dependence of dissolved thickness of tungsten plates on CO_2 partial pressure in molten Na_2CO_3 at 1173 K for 2.5 h. (b) IR spectrum of the exhaust gas of the oxidative dissolution experiment of tungsten under Ar–CO_2(0.2 atm) atmosphere in molten Na_2CO_3 at 1173 K.

Fig. 7 Calculated potential–p_{CO_2} diagram from the reported thermodynamic data for W species (Red line) and WC species (Orange line) in molten Na_2CO_3 at 1173 K from the reported thermodynamic data.[48,49] (Blue line) Stable region of molten Na_2CO_3. The solid and dotted color lines correspond to equilibriums at the activity of WO_4^{2-} ion to be 10^{-2} and 10^{-4}, respectively.

Fig. 8 Schematic illustration of the reaction scheme of oxidative dissolution of tungsten metal in molten Na_2CO_3 by (a) O_2^{2-}/O_2^{-} ions and (b) CO_3^{2-} ions

Fig. 9 Dependence of dissolution thickness of tungsten plates on CO_2 partial pressure in molten Na_2CO_3 at 1173 K in Ar–O_2(0.2 atm)–CO_2 atmosphere for 2.5 h.

Fig. 10 Cyclic voltammograms for Au wire electrode in (a) Ar–O_2(0.2 atm)–CO_2(6×10^{-4} atm) and (b) O_2(0.2 atm)–CO_2(0.8 atm) in molten Na_2CO_3 at 1173 K. Scan rate: 0.1 V s^{-1}. (A) O_2 evolution, (B) O_2 reduction, (C) CO_3^{2-} reduction, (D) Na gas evolution, and (E) C deposition.

590

591 Table 1 Standard Gibbs energy of formation at 1173 K.[48,49]

592

Species	ΔG°_{f} / kJ mol^{-1}	Reference
Na_2CO_3(l)	–809.612	[48]
Na_2O(s)	–254.073	[48]
Na_2O(l)	–245.637	[48]
CO_2(g)	–396.072	[48]
CO(g)	–215.458	[48]
C(s)	0	[48]
O_2(g)	0	[48]
Na(g)	0	[48]
W(s)	0	[49]
WC(s)	–35.371	[49]
Na_2WO_4(l)	–1109.712	[49]
WO_3(s)	–543.810	[49]

593

594

595

596 Table 2 Standard Gibbs energy of formation for ionic species at 1173 K.[48,49]

597

Species	ΔG°_{f} / kJ mol^{-1}
O^{2-}(l)	0
CO_3^{2-}(l)	–563.975
O_2^{2-}(l)	2.615 [a]
O_2^{-}(l)	29.497 [a]
Na^{+}(l)	–122.819
WO_4^{2-}(l)	–864.075

598 a: Calculated by applying the molar ratio of $O^{2-}/O_2^{2-}/O_2^{-}$ equilibrium in molten Na_2CO_3 at 1200 K
599 to 1173 K.

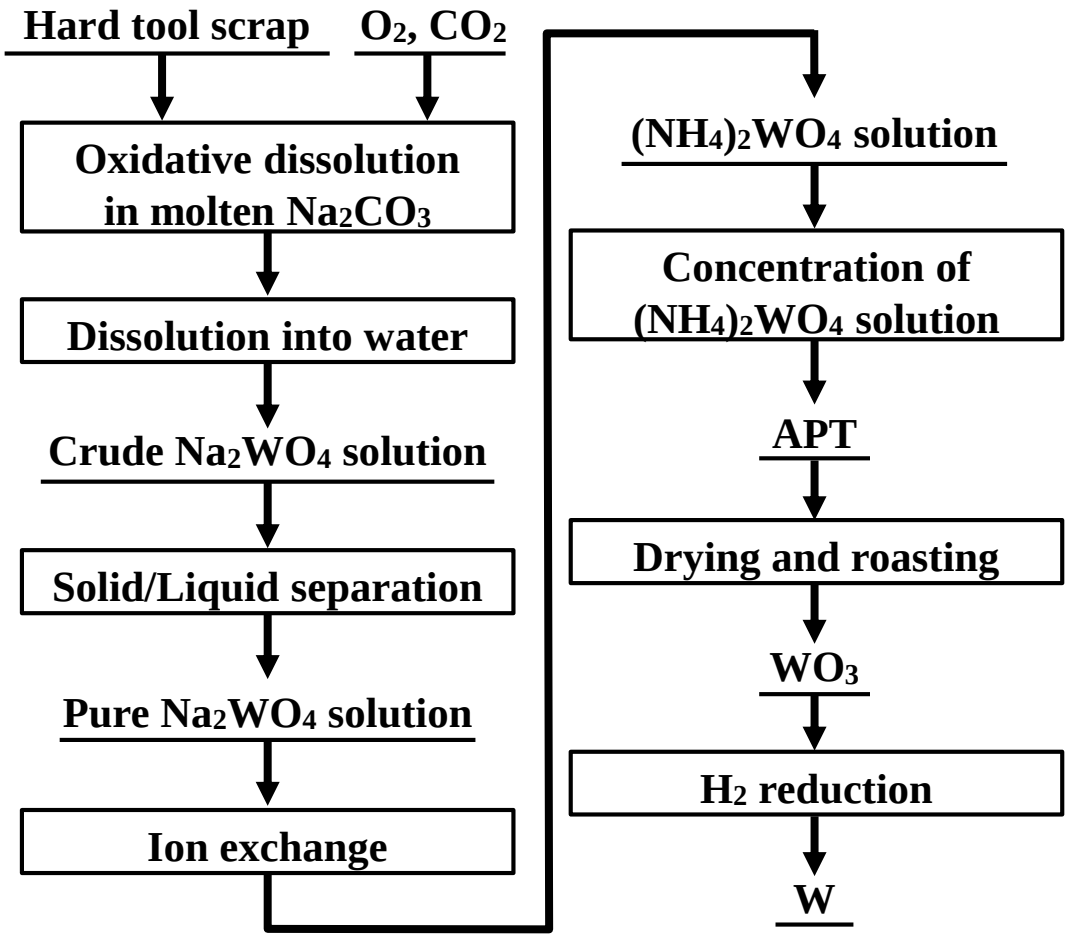

APT:
$(NH_4)_{10}(H_2W_{12}O_{42})\cdot 4H_2O$

Figure 1 Flowchart of molten carbonate method for recycling of tungsten proposed in this study.

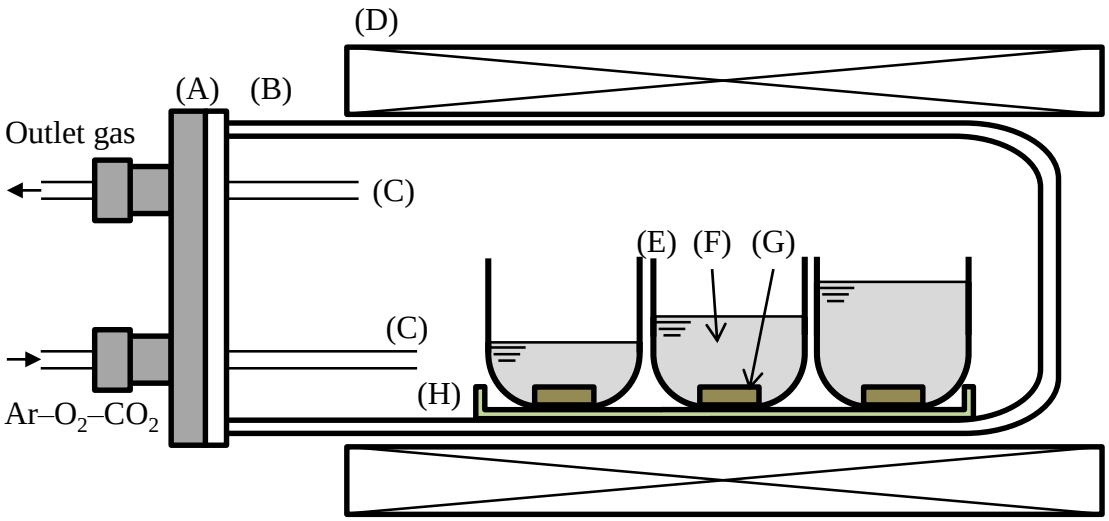

Figure 2 Schematic drawing of oxidative dissolution experiment of tungsten metal at 1173 K. (A) Stainless steel lid, (B) SiO_2 reaction tube, (C) alumina tube, (D) electric furnace, (E) alumina crucible, (F) molten Na_2CO_3, (G) W plate, and (H) Au plate.

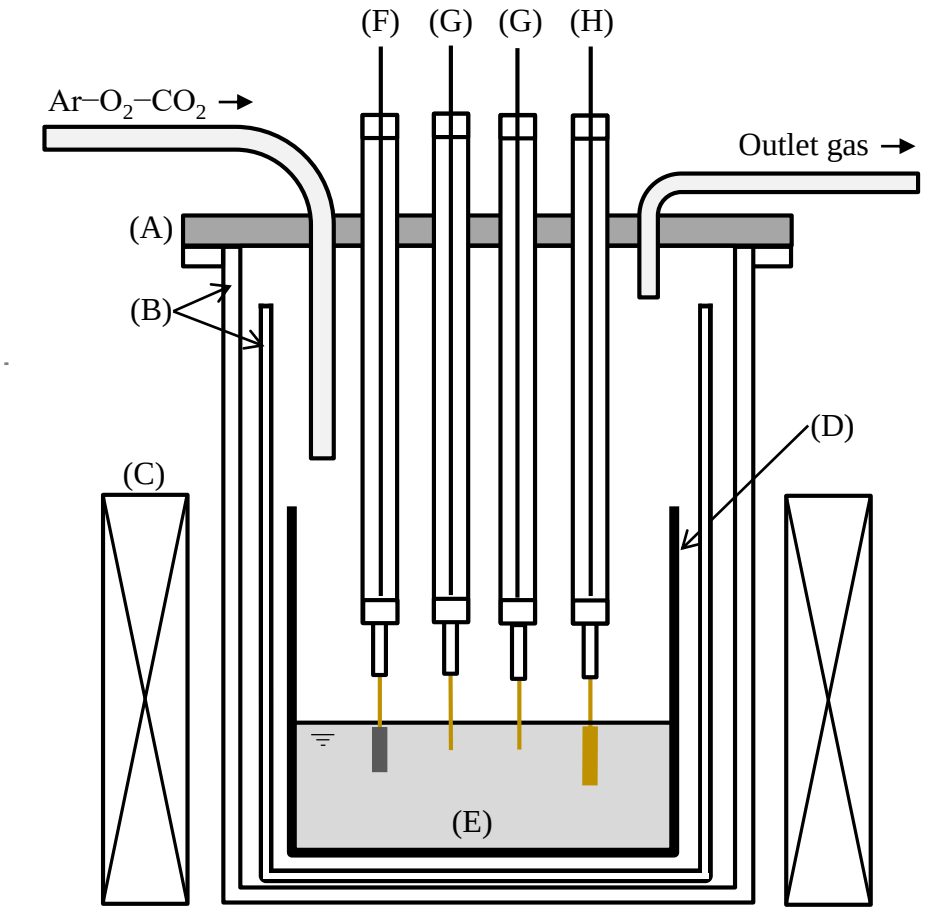

Figure 3 Schematic drawing of electrochemical measurement of tungsten metal at 1173 K. (A) Stainless steel lid, (B) SiO_2 reaction tube, (C) electric furnace, (D) alumina crucible, (E) molten Na_2CO_3, (F) W plate electrode, (G) Au wire electrode, and (H) Au plate electrode.

(a) Salt

(b) W plate

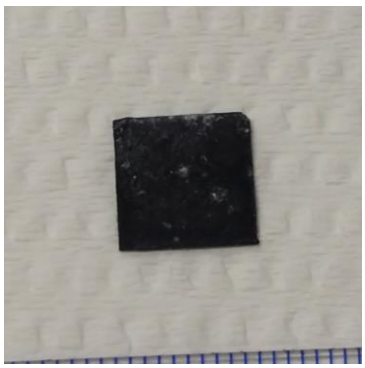

(c) XRD (salt)

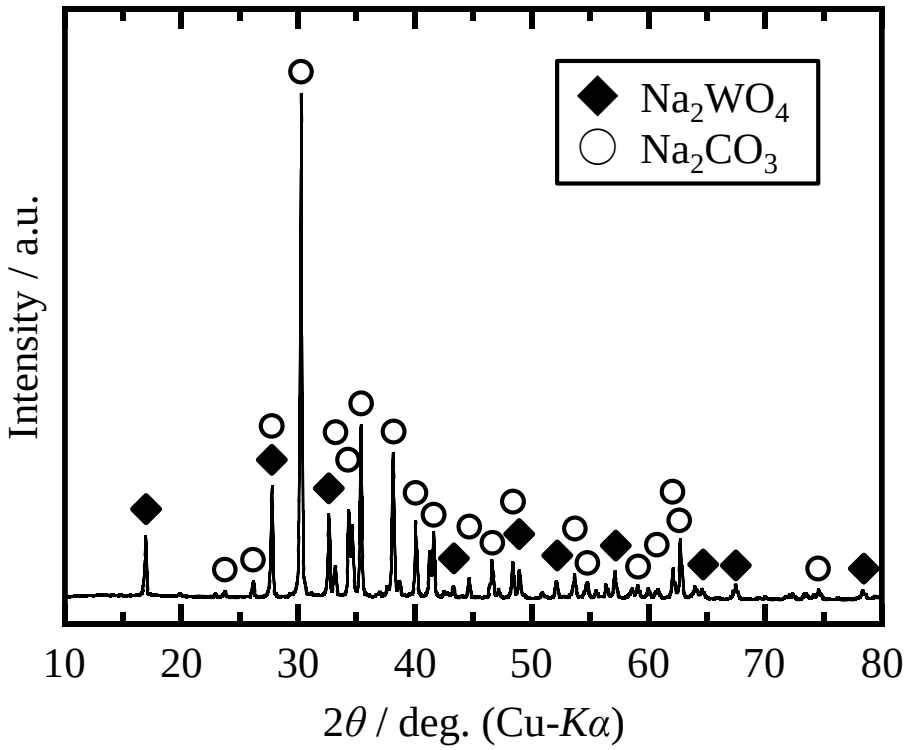

Figure 4 Representative appearance of (a) the recovered salt and (b) W plate, and (c) XRD pattern of the salt after oxidative dissolution experiment of tungsten plate for 2.5 h in molten Na_2CO_3 with 6-mm melt depth at 1173 K in Ar–O_2(0.2 atm)–CO_2(6×10^{-4} atm) atmosphere.

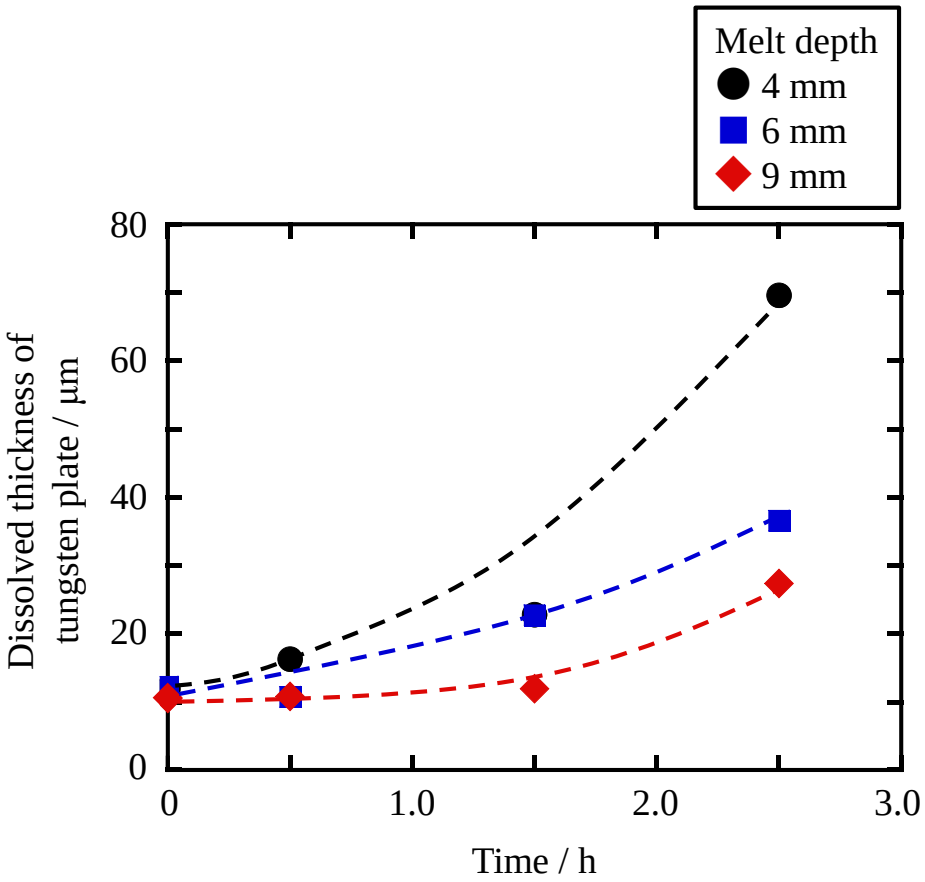

Figure 5 Dissolved thickness of tungsten plates in molten Na_2CO_3 at 1173 K in Ar–O_2(0.2 atm)–CO_2(6 × 10^{-4} atm) atmosphere.

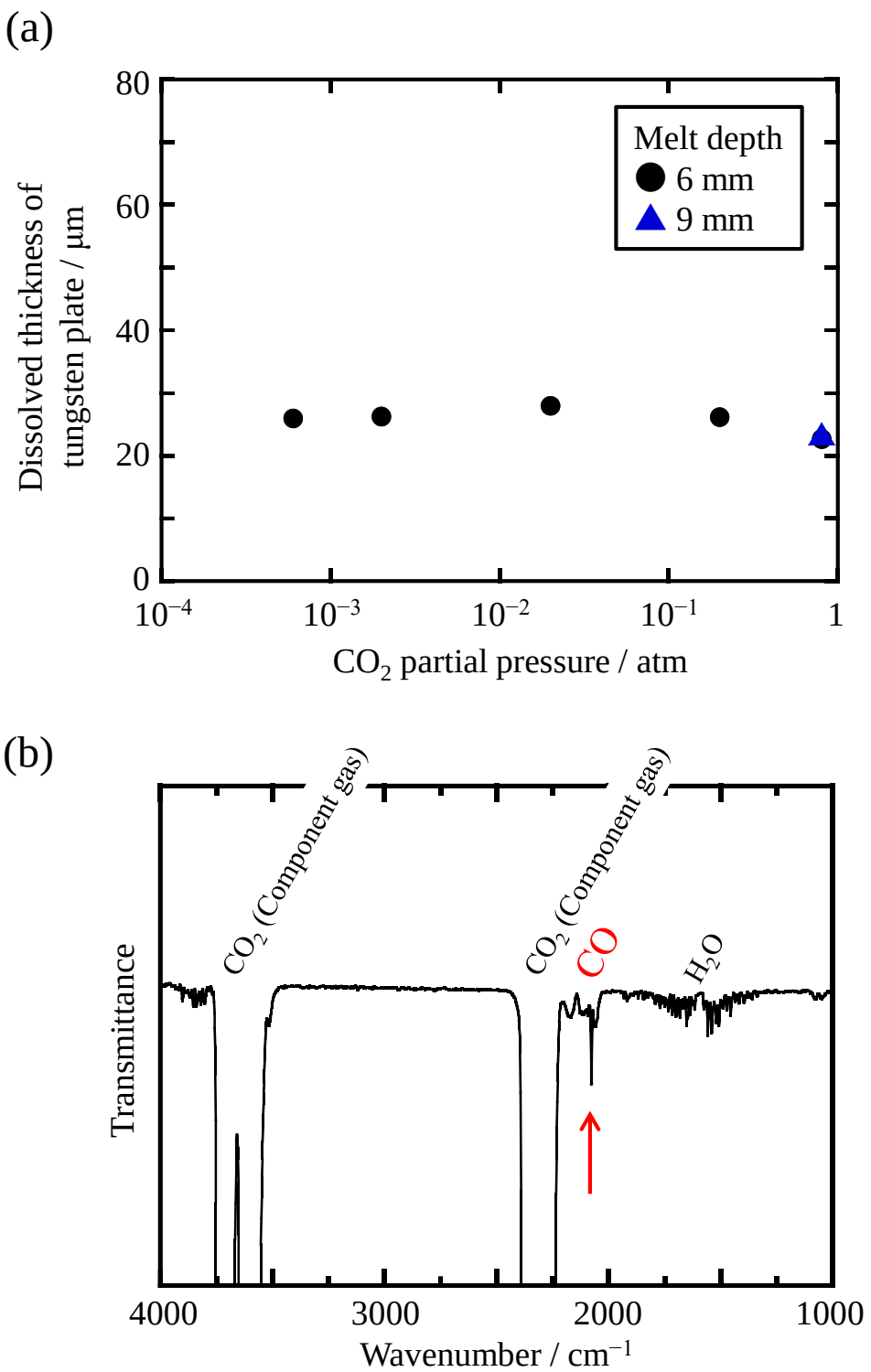

Figure 6 (a) Dependence of dissolved thickness of tungsten plates on CO_2 partial pressure in molten Na_2CO_3 at 1173 K for 2.5 h. (b) IR spectrum of the exhaust gas of the oxidative dissolution experiment of tungsten under Ar–CO_2(0.2 atm) atmosphere in molten Na_2CO_3 at 1173 K.

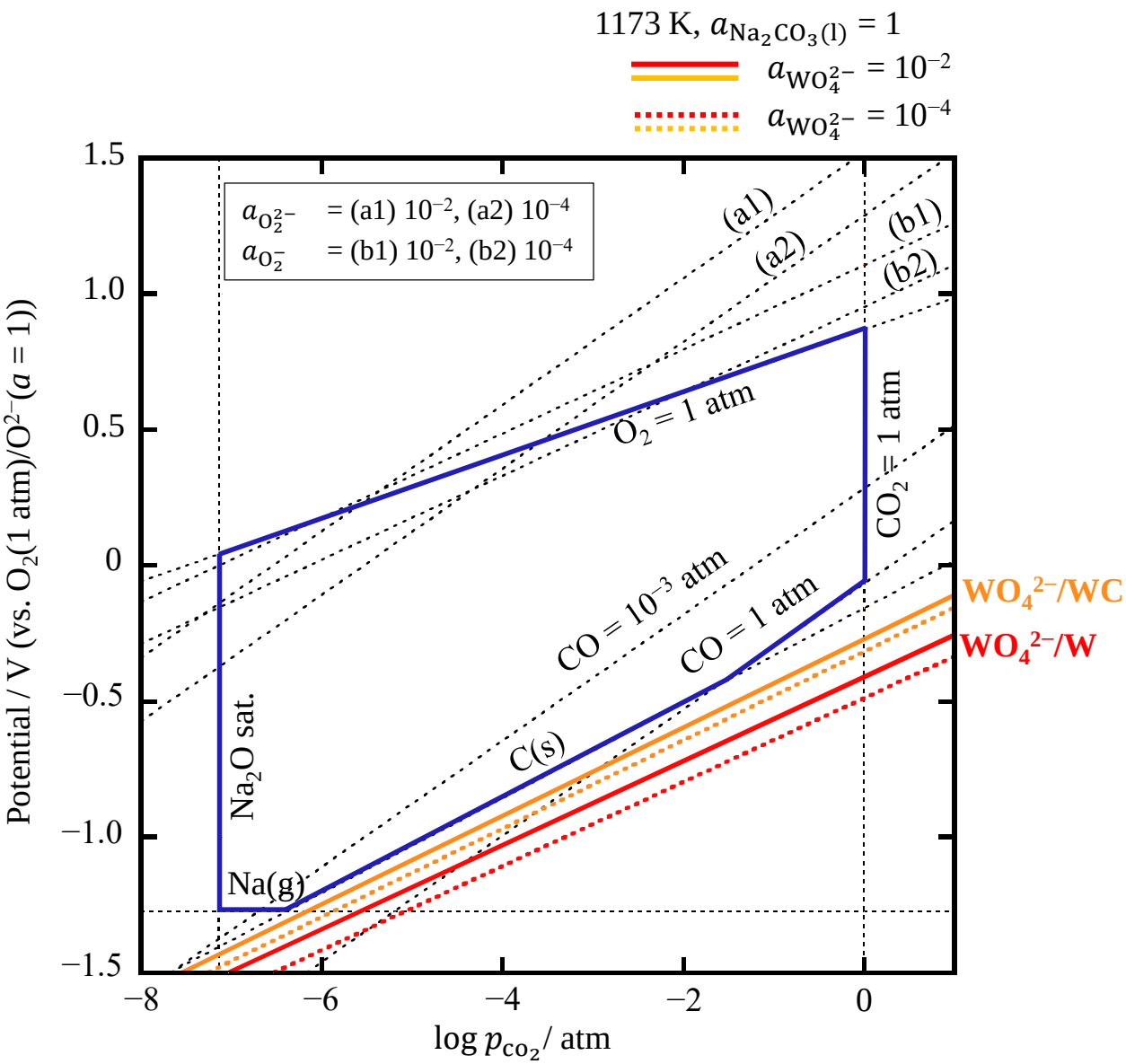

Figure 7 Calculated potential–p_{CO_2} diagram from the reported thermodynamic data for W species (Red line) and WC species (Orange line) in molten Na_2CO_3 at 1173 K from the reported thermodynamic data.[31,32] (Blue line) Stable region of molten Na_2CO_3. The solid and dotted color lines correspond to equilibriums at the activity of WO_4^{2-} ion to be 10^{-2} and 10^{-4}, respectively.

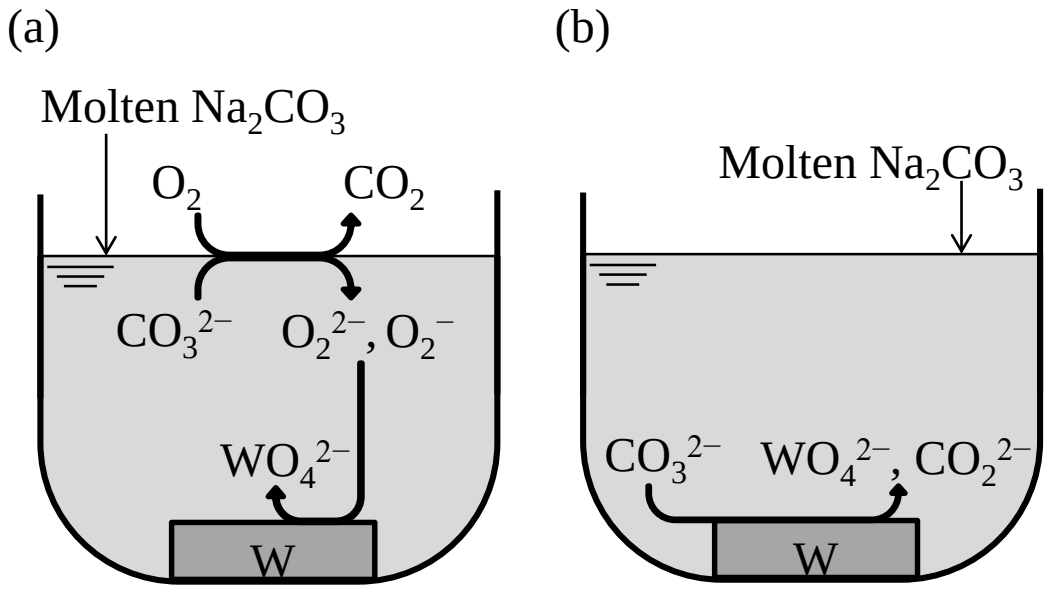

Figure 8 Schematic illustration of the reaction scheme of oxidative dissolution of tungsten metal in molten Na_2CO_3 by (a) O_2^{2-}/O_2^- ions and (b) CO_3^{2-} ions

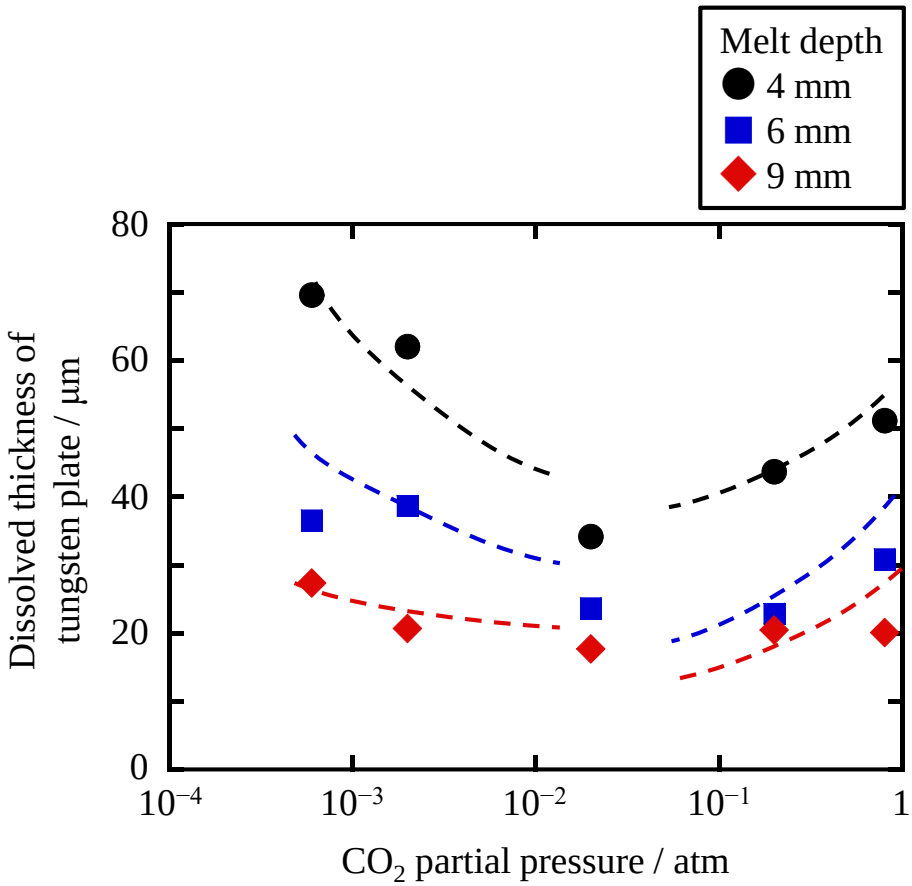

Figure 9 Dependence of dissolved thickness of tungsten plates on CO_2 partial pressure in molten Na_2CO_3 at 1173 K in Ar–O_2(0.2 atm)–CO_2 atmosphere for 2.5 h.

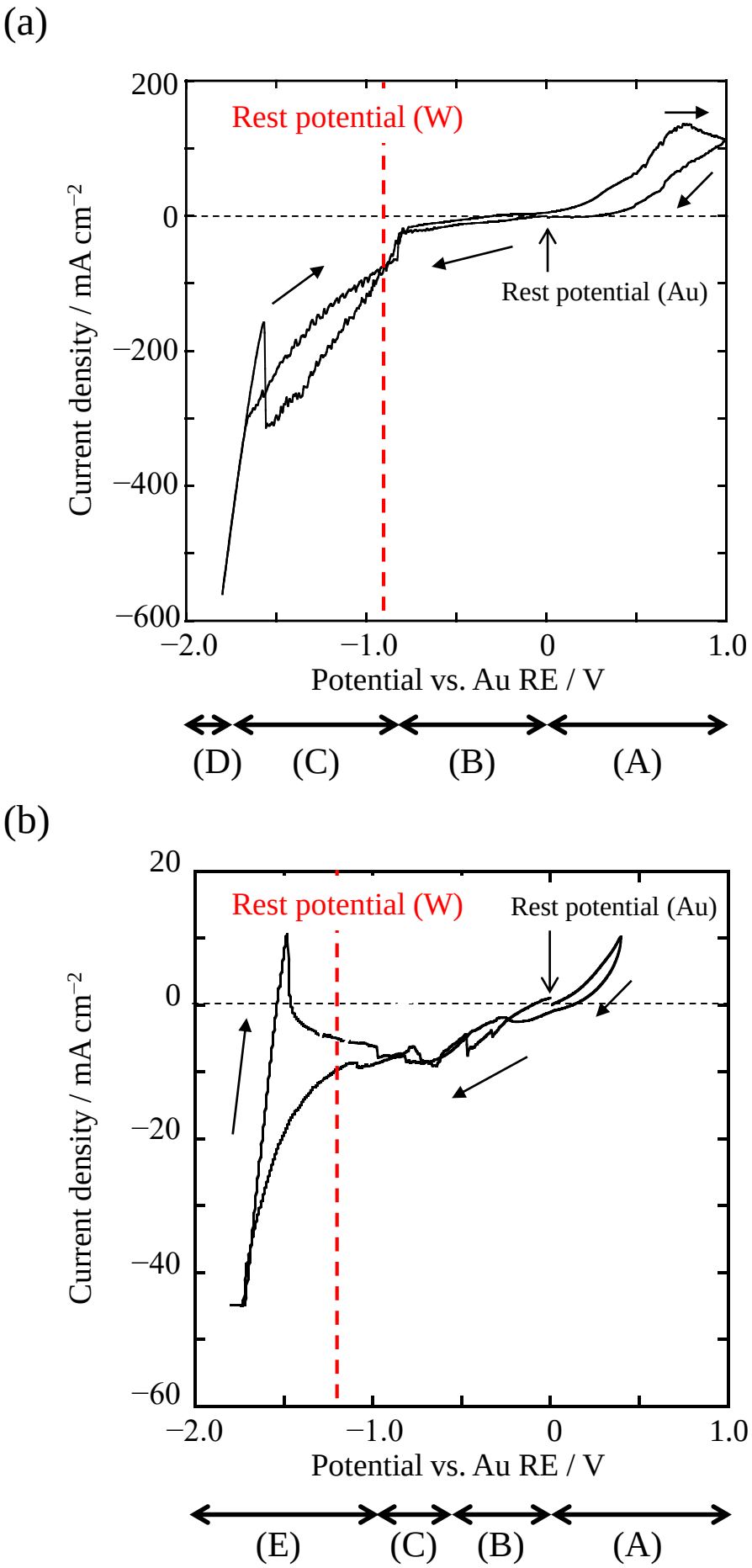

Figure 10 Cyclic voltammograms for Au wire electrode in (a) Ar–O_2(0.2 atm)–CO_2(6 × 10^{-4} atm) and (b) O_2(0.2 atm)–CO_2(0.8 atm) in molten Na_2CO_3 at 1173 K. Scan rate: 0.1 V s^{-1}. (A) O_2 evolution, (B) O_2 reduction, (C) CO_3^{2-} reduction, (D) Na gas evolution, and (E) C deposition.